Theor Chem Acc (2012) 131:1276
DOI 10.1007/s00214-012-1276-x

REGULAR ARTICLE

The influence of carbon dioxide cosolvent on solubility in poly(ethylene glycol)

Michael T. Huber · John M. Stubbs

Received: 31 August 2012 / Accepted: 4 September 2012 / Published online: 22 September 2012

Abstract Supercritical carbon dioxide (CO_2) and poly(ethylene glycol) (PEG) can be utilized as an environmentally friendly biphasic solvent system for catalysis reactions and subsequent product separation. To efficiently implement this technology, it is important to understand how solutes partition between these phases as well as how dissolved CO_2 in PEG affects the solvent properties. The work presented here explores the influence of CO_2 on the solubility of four different solutes in PEG. The transferable potentials for phase equilibria-united atom force field and configurational-bias Monte Carlo molecular simulation were employed to determine the solubilities of ethylbenzene, 1-octene, 1-pentanol, and 2-pentanone at 323.15 K and 15 MPa in PEG-600 using an ideal vapor phase with a Poynting-corrected vapor pressure. The effect of CO_2 concentration within the PEG phase was determined by varying the amount from no CO_2 to the saturation limit. The results indicate that while there is preferential solvation of CO_2 around the solutes, solubility of non-polar solutes is unchanged whereas there is a modest increase for polar solutes as the concentration of CO_2 increases. Increased solubility is analyzed in terms of both modified solvent structure and direct solute–CO_2 interactions.

Keywords Poly(ethylene glycol) · Supercritical carbon dioxide · Solvation · Monte Carlo simulation

Published as part of the special collection of articles derived from the conference: Foundations of Molecular Modeling and Simulation 2012.

M. T. Huber · J. M. Stubbs (✉)
Department of Chemistry and Physics, University of New England, 11 Hills Beach Road, Biddeford, ME 04005, USA
e-mail: jstubbs@une.edu

1 Introduction

Recently, several green reaction systems that minimize the use of traditional organic solvents have been discussed in the literature that include homogeneous catalysis in poly(ethylene glycol) (PEG) followed by reaction product separation with supercritical carbon dioxide (CO_2) [1–7]. Because the efficiency of the separation of reaction products is dependent upon knowledge of the phase behavior of the relevant substances together with PEG and CO_2, knowledge of this phase behavior allows predictions of product partitioning to be made which are integral to the design of a separation scheme. A complication for these predictions is that carbon dioxide can dissolve in PEG, up to substantial quantities (20–30 % CO_2 by mass) depending upon temperature, pressure, and PEG molecular weight [8–11], and can thus considerably change the solvent environment experienced by the solutes that are extraction targets. Thus, experimental data for a given compound's solubility in PEG may or may not be applicable to the ternary system created upon addition of CO_2.

As our previous work [12] shows the importance of CO_2 solvation of ethylbenzene in PEG at pressures of 10–20 MPa and temperatures of 308.15–348.15 K, the goal of this present study is to calculate the effect of dissolved CO_2 within PEG on the solubility of four solutes with varying degrees of polarity, possibility of hydrogen bond formation, and rigidity/flexibility under similar pressure and temperature conditions. Thus, building off our previous work, we report here the study of the solubility of two non-polar solutes, ethylbenzene (EB) and 1-octene (OCT), each with eight carbon atoms; OCT was also chosen because there is experimental data available for the PEG + CO_2 + 1-octene system at comparable temperatures, though somewhat lower pressures [13]. For comparison,

we also studied two polar solutes, 1-pentanol (POL) and 2-pentanone (PNE). POL was chosen due to its having a similar normal boiling point as compared to EB while PNE was chosen due to its similar size to POL and lack of hydrogen bond donor functionality. All four compounds were studied individually as solutes in PEG + CO_2 at the calculated CO_2 solubility limit, S, at $\frac{2}{3}S$, and at $\frac{1}{3}S$ as well as with no CO_2 present.

2 Methods

All molecules were modeled using the transferable potentials for phase equilibria-united atom (TraPPE-UA) forcefield for alkenes, alkanols, alkanones, arenes, and PEG [14–16], together with the CO_2 model of Siepmann and Potoff [17]. This forcefield has an interaction site for every atom except for hydrogen atoms directly bonded to a carbon atom, which are represented with a single pseudo-atomic site, was fit to small molecule phase equilibria, and is designed to reproduce experimental *PVT* behavior over a wide range of conditions. All bonded interactions are modeled with rigid bond lengths, harmonic bending for sites separated by two bonds, and for sites separated by three bonds both torsional interactions, made up of a cosine series, and electrostatic interactions, that, when present, are scaled by half. Sites separated by four or more bonds or on different molecules interact via the Lennard-Jones and Coulomb potentials. Finally, intramolecular interactions between a hydroxyl-hydrogen and an oxygen atom separated by exactly four bonds contain a short-range repulsive interaction.

The *NPT* Gibbs ensemble [18–20] with one box containing PEG + CO_2 and another a solute reservoir was employed for phase equilibrium calculations at $T = 323.15$ K and $P = 15$ MPa. An Ewald summation with $\kappa \times L = 5$, $K_{max} = 6$ and tin-foil boundary conditions was employed for electrostatic interactions while analytic tail corrections were used beyond the cutoff distance of 12 Å for long-range interactions for the Lennard-Jones potential [21]. In addition to standard Monte Carlo moves of rotation, translation, and volume displacement, coupled-decoupled configurational-bias Monte Carlo (CBMC) [22–25] and self-adapting fixed endpoint CBMC [26] moves were used to sample conformational degrees of freedom of flexible molecules. Molecule exchange between the polymer-rich box and an ideal vapor phase for the solute with a chemical potential equal to that of the pure solute liquid at the same T and P allowed the determination of solubility within the PEG + CO_2 box. The ideal vapor phase was chosen as it is thermodynamically equivalent to the liquid, yet increases simulation efficiency by avoiding having to insert solute molecules into a dense liquid solute phase as part of the chemical potential equilibrium. Using the Poynting-corrected vapor pressure for the solute vapor phase allows this approach to be implemented, where

$$P_{corr} = P_{coex} \exp\left(\frac{\bar{V}_l(P_{ext} - P_{coex})}{RT}\right) \quad (1)$$

and P_{corr}, P_{coex}, and P_{ext} are the Poynting-corrected vapor pressure, the equilibrium vapor pressure at T, and the external pressure, respectively, and $\bar{V}_l, R$, and T are the molar volume of the liquid solute at 323.15 K and P_{coex}, the ideal gas constant, and the absolute temperature, respectively [27, 28].

PEG-600 is represented as monodisperse molecules containing 13 repeat units, that is, $HO(CH_2CH_2O)_{13}H$. For each system, the polymer phase contains 35 PEG-600 molecules and either 0, 33, 66, or 99 CO_2 molecules while the vapor phase initially contained 60 solute molecules with at least 3.5×10^6 and 2×10^6 Monte Carlo (MC) cycles used for equilibration and production, respectively, where 1 MC cycle consists of $N_{molecule}$ MC moves. For the calculation of the solubility of CO_2 in PEG, 35 PEG-600 molecules and 400 CO_2 molecules were simulated in the *NPT* Gibbs ensemble at 323.15 K and 15 MPa. These preliminary simulations indicated that for these models, the solubility of CO_2 in PEG-600 at these conditions is a molality of $S = 4.8$ mol kg^{-1} which corresponds to 99 CO_2 molecules per 35 PEG-600 molecules. Thus, the four different amounts of CO_2 considered in this study are $N_{CO_2} = 99$ corresponding to $m = S = 4.8$ mol kg^{-1}; $N_{CO_2} = 66$ corresponding to $m = \frac{2}{3}S = 3.2$ mol kg^{-1}; $N_{CO_2} = 33$ corresponding to $m = \frac{1}{3}S = 1.6$ mol kg^{-1} and finally without any CO_2. For all state points studied here, four independent simulations were carried out which allowed the determination of statistical uncertainties.

3 Results and discussion

3.1 Solubility

The solubility of each solute in the PEG + CO_2 systems is given in Table 1. For all systems investigated here, the solubility of polar solutes is higher than that of the non-polar solutes, consistent with PEG being a polar molecule.

For the non-polar solutes, as the amount of CO_2 increases, the solubility stays unchanged or decreases slightly, possibly due to space that would otherwise be available to solutes being instead occupied by CO_2. The higher solubility of EB relative to OCT is consistent with it having a more compact shape. The solubility of OCT in PEG-600 at 323.15 K and 15 MPa without CO_2 from this

Table 1 Solubility in molecules nm^{-3} in PEG + CO_2 mixtures

Solute	CO_2 concentration			
	0	$\frac{1}{3}S$	$\frac{2}{3}S$	S
EB	0.19_4	0.14_2	0.19_4	0.16_1
OCT	0.14_5	0.10_2	0.08_2	0.12_2
POL	0.55_4	0.59_5	0.63_5	0.61_9
PNE	0.49_5	0.47_9	0.48_4	0.62_4

work is 2.4 ± 0.9 mass % and compares very favorably to that reported by Li et al. [13] as 2.50 mass % at 318.15 K and 3.30 mass % at 328.15 K and 0.1 MPa in neat PEG-600; at a CO_2 concentration of S, the result of 2.0 ± 0.3 mass % at 323.15 K and 15 MPa also compares favorably to reported values of 3.10 mass % at 318.15 K and 9.13 MPa and 3.90 mass % at 328.15 K and 9.13 MPa given that the experimentally observed trend is for mass % of OCT to decrease as pressure increases. For polar solutes, the solubility increases as the amount of CO_2 increases, up to 11–27 % at the CO_2 solubility limit, S, as compared to without CO_2 present. One possible explanation includes direct solute interactions with CO_2 enhancing solubility; alternately, it may be that the structure of the PEG phase is being altered to increase favorable electrostatic interactions between the solute and PEG. As discussed further below in Sect. 3.2, the results suggest a combination of these two possibilities. The densities of the PEG + CO_2 + solute phases are all similar and are in the range of 1.09–1.11 g cm^{-3}. As the mass increases due to addition of CO_2, this constant density indicates that there is a modest amount of polymer swelling to accommodate the CO_2 and maintain a constant density.

3.2 Structural analysis

The solute–solute center-of-mass (COM) radial distribution functions (RDFs), $g(r)$, shown in Fig. 1 all have a modest initial peak around 5–6 Å, dropping off at larger distances. The corresponding number integrals (NIs), $N(r)$, indicate that on average there is one-half neighbor within this distance for the polar solutes and less than that for the non-polar solutes. This indicates that there is not a strong tendency for the solutes to associate with each other while dissolved in the PEG + CO_2 phase and that they are mostly distributed throughout the polymer phase.

There is little change in the hydrogen bonding interactions of the polymer terminal hydroxyl groups with each other, as indicated by the lack of change in the oxygen-oxygen RDF curves in Fig. 2a for results with POL as solute, which would be expected out of all the solutes to potentially have the largest impact on PEG hydrogen bonding. All other solute systems have comparable curves

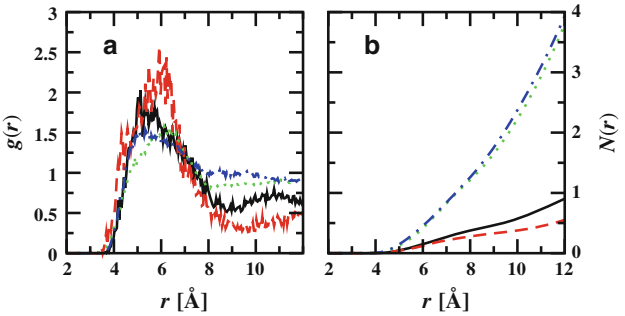

Fig. 1 **a** Solute–solute COM RDFs for ethylbenzene (*solid*), 1-octene (*dashed*), 1-pentanol (*dotted*) and 2-pentanone (*dash-dotted*) in PEG-600 at 4.8 mol $kg^{-1}CO_2$, and **b** corresponding number integrals

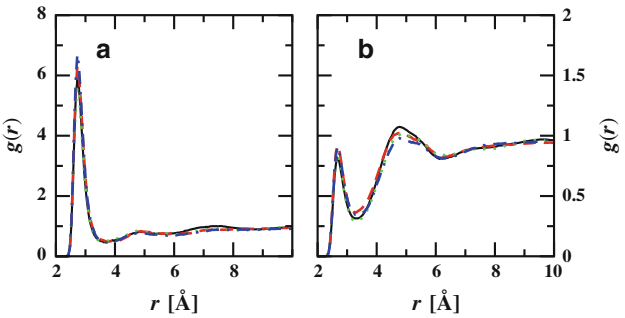

Fig. 2 **a** PEG hydroxyl-oxygen to PEG hydroxyl-oxygen RDFs with 1-pentanol as solute as a function of increasing CO_2 concentration with *solid*, *dashed*, *dotted* and *dash-dotted lines* corresponding to 0, 1.6, 3.2 and 4.8 mol kg^{-1}, respectively, **b** PEG hydroxyl-oxygen to PEG ether-oxygen RDFs with 1-pentanol as solute with line styles as in (**a**)

(not shown). For comparison, the RDFs for the hydroxyl-oxygen–ether oxygen sites, given in Fig. 2b, show a shift to larger r for the second peak as the concentration of CO_2 increases, consistent with polymer swelling upon addition of CO_2.

Figure 3 shows CO_2–CO_2 and CO_2-solute COM RDFs and Fig. 4 the corresponding NIs. For all solutes, the largest changes in the radial distribution functions occur between the lowest concentration of CO_2, $\frac{1}{3}S$, and the higher concentrations. All NIs have CO_2 around itself as higher initially, corresponding to its smaller size, and are then surpassed by CO_2 around solute between 5 and 6 Å, indicating a solvation structure of CO_2 around the solutes while in the polymer phase. This solvation shell is likely incomplete at $\frac{1}{3}S$ leading to the differences in RDFs for higher CO_2 concentrations, while at $\frac{2}{3}S$ the CO_2 solvation shell is mostly in place.

For polar solutes, the NIs show a drop on the CO_2 around solute curves at increasing distance particularly for higher CO_2 concentrations. This depletion, taken together with the increasing solubility under these conditions, is consistent with close interactions between the solute and

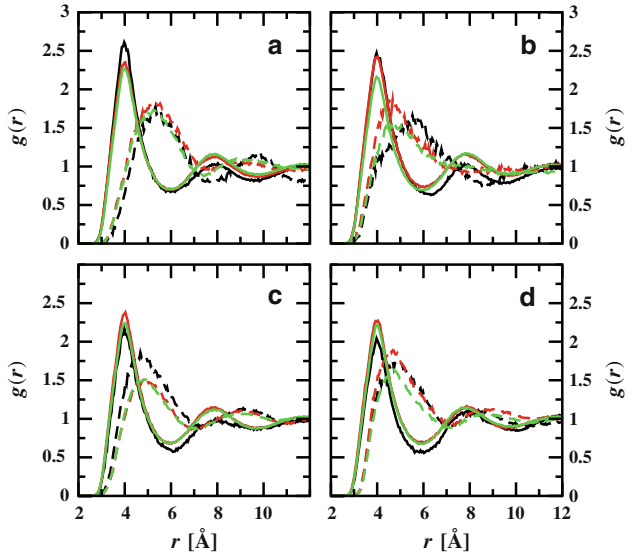

Fig. 3 COM RDFs for CO_2 around CO_2 (*solid lines*) and around solute (*dashed lines*) with *black*, *dark* and *light* corresponding to initial carbon dioxide concentrations of 1.6, 3.2 and 4.8 mol kg^{-1}, respectively, for **a** ethylbenzene, **b** 1-octene, **c** 1-pentanol, and **d** 2-pentanone

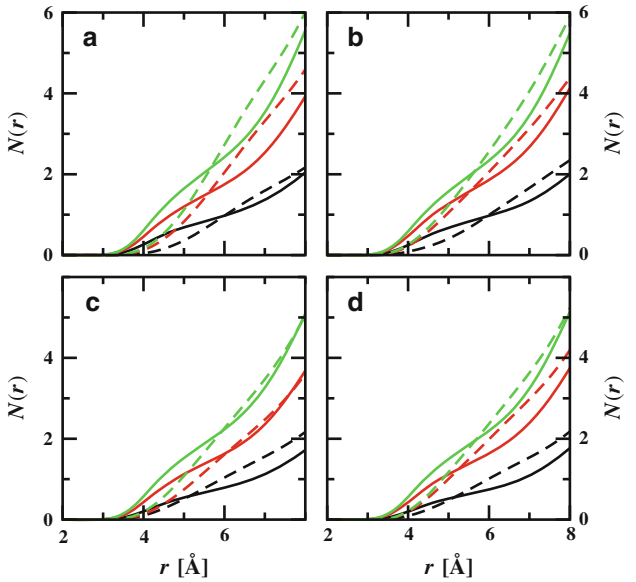

Fig. 4 COM NIs for **a** ethylbenzene, **b** 1-octene, **c** 1-pentanol, and **d** 2-pentanone with line styles as in Fig. 3

PEG, leading to a solvation structure with more polymer adjacent to the solute than in the non-polar solute case.

To investigate the polar solutes more completely, we turn to their site-site RDFs and NIs for more detail. For analysis of POL's hydrogen bonding in terms of what oxygen is acting as a hydrogen bond acceptor for its hydroxyl-hydrogen, all four unique types of oxygen atoms were considered: other POL oxygens; PEG hydroxyl-oxygens, O_A; PEG ether-oxygens, O_E; and finally CO_2 oxygens. To characterize this, RDFs and their corresponding NIs are shown in Figs. 5 and 6, respectively. Since the initial peak in the RDFs corresponds to a hydrogen bond, the minimum between the first two peaks can be used as a distance criterion to identify a hydrogen bond. Using this definition, a hydrogen bond is present if the hydrogen-oxygen distance is less than or equal to 2.5 Å $=r_{HB}$. Looking at the number of oxygen neighbors at that

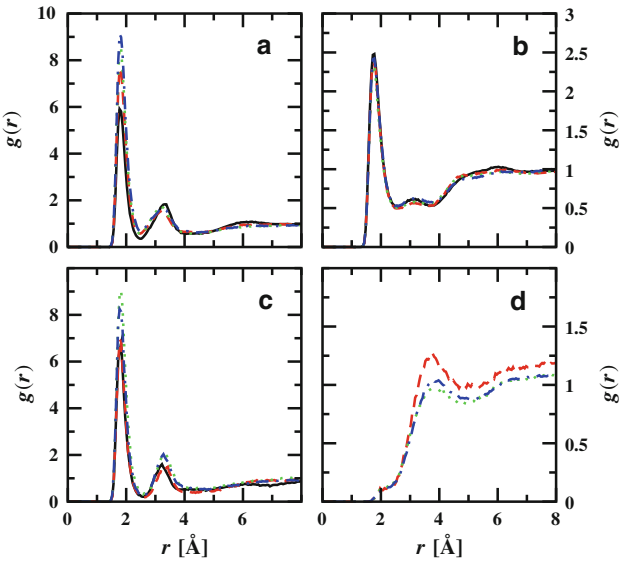

Fig. 5 RDFs for 1-pentanol hydroxyl-hydrogen to **a** PEG hydroxyl-oxygen, **b** PEG ether-oxygen, **c** 1-pentanol oxygen, and **d** CO_2 oxygen as a function of CO_2 concentration with *solid*, *dashed*, *dotted* and *dash-dotted lines* corresponding to 0, 1.6, 3.2 and 4.8 mol kg^{-1}, respectively.

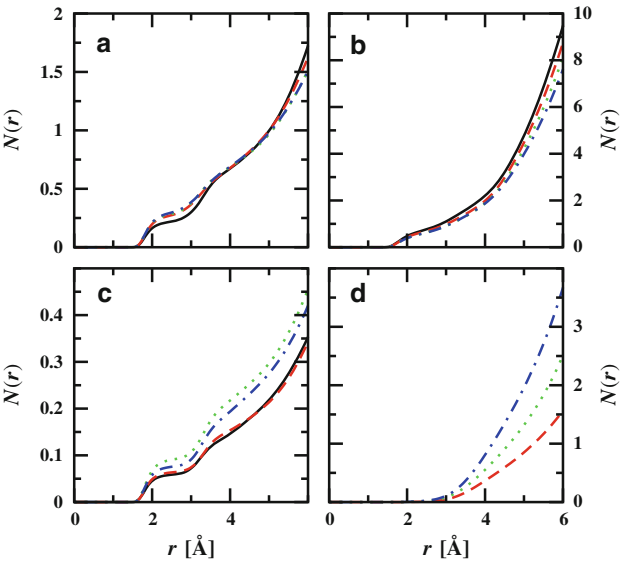

Fig. 6 NIs for 1-pentanol hydroxyl-hydrogen to **a** PEG hydroxyl-oxygen, **b** PEG ether-oxygen, **c** 1-pentanol oxygen, and **d** CO_2 oxygen as a function of CO_2 concentration with line styles as in Fig. 5

cutoff value from the NIs, the hydrogen bonding to other solutes is slightly dependent on the concentration of CO_2; the number to CO_2 is negligible compared with the others (0.025 at the highest CO_2 concentration); finally, it is apparent that most of the hydrogen bonds are to PEG. For a given hydroxyl-hydrogen, the sum of the NIs of all four oxygen types at r_{HB} is ≈ 1.0 at all CO_2 concentrations indicating that essentially all of them are participating in a hydrogen bond. Interestingly, as the amount of CO_2 increases, the number of hydrogen bonds to O_E sites drops while the number to O_A sites increases. As the O_A site has a larger partial charge, it is not surprising that this is a preferred site, despite there being six times as many O_E sites. However, the ability of POL molecules to switch hydrogen bond acceptor sites with the addition of CO_2 to the more energetically favorable site is unexpected and indicates that additional CO_2 is affecting the PEG + CO_2 solution structure to make this switch possible. We hypothesize this is due to CO_2-induced swelling of PEG which initially frees up space around PEG O_A sites as it fills in with CO_2, after which the CO_2 can be displaced with POL which prefers this more favorable binding site. PEG expansion upon addition of CO_2 has been previously reported and can be substantial, up to a 35 % volume increase, depending on pressure, temperature, and PEG molecular weight [11, 29].

While PNE also shows enhanced solubility as CO_2 concentration increases, the mechanism must differ from that described above for POL as PNE does not have a hydrogen bond donor site. As its ketone oxygen, O_K, is negatively charged, there are electrostatic interactions with the positive charges in the system. With no or little CO_2 present, the principal positively charged sites are the CH_2 groups in PEG, while as the amount of CO_2 increases, its carbon site, with a charge greater than that of the CH_2 sites, is also available for interaction. The site-site RDFs and NIs for O_K and PEG interior-CH_2 sites as well as for O_K and CO_2 carbon sites are shown in Fig. 7. RDFs and NIs for O_K to PEG terminal-CH_2 sites (not shown) are analogous to those for PEG interior-CH_2 sites. As can be seen in the NIs, the number of CH_2s drops and number of CO_2 carbons increases as CO_2 concentration increases, as is expected. Yet, the CH_2 NI drop is not as low as the drop in O_K to O_E NIs (not shown), where this pair can be used as a measure of structural change due to polymer swelling. This indicates that there is still some preferential interaction between O_K and CH_2 even as the concentration of CO_2 increases. Similarly, O_K to CO_2 carbon NIs rise considerably from $\frac{1}{3}S$ to $\frac{2}{3}S$, by approximately the expected factor of two, while from $\frac{2}{3}S$ to S, the increase is not the expected factor of 1.5 but rather only approximately 1.2, indicating that the amount of CO_2 at $\frac{2}{3}S$ is close to sufficient for the desired solvation shell of PNE. This is consistent with the interpretation of the COM NIs of CO_2 around PNE as described above.

3.3 Local solvation

To further explore the composition of the solvation shell of each solute, the local CO_2 site fraction, $x(r)$, around a solute's COM is plotted in Fig. 8, where

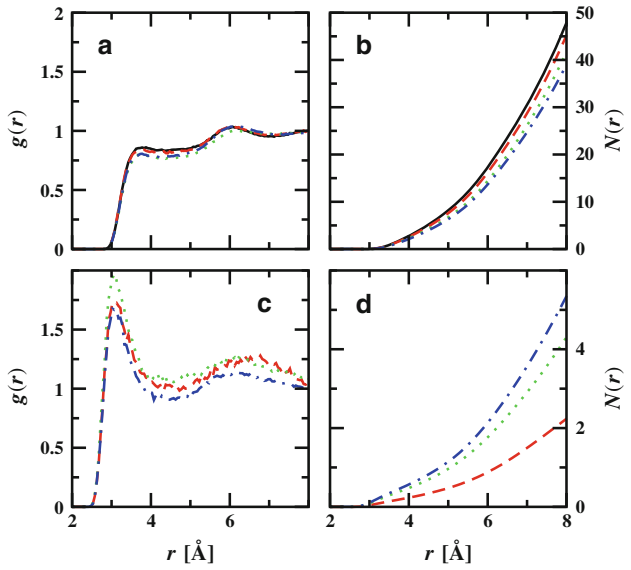

Fig. 7 2-pentanone-oxygen to PEG interior-CH_2 **a** RDFs, and **b** corresponding NIs and 2-pentanone-oxygen to CO_2 carbon, **c** RDFs, and **d** corresponding NIs as a function of CO_2 concentration with line styles as in Fig. 6

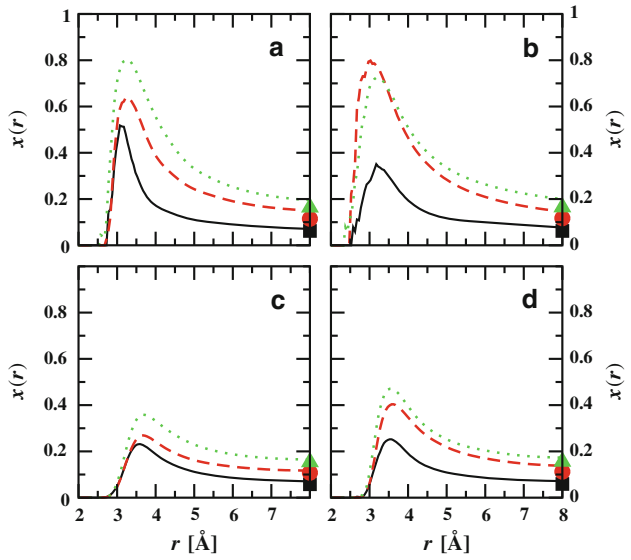

Fig. 8 Local CO_2 site fraction, $x(r)$, (*lines*) and bulk CO_2 site fractions (*symbols*) as a function of CO_2 concentration with *solid line* and *squares*, *dashed lines* and *circles*, and *dotted lines* and triangles corresponding to 1.6, 3.2 and 4.8 mol kg^{-1}, respectively, for **a** ethylbenzene, **b** 1-octene **c**, 1-pentanol, and **d** 2-pentanone

$$x(r) = \frac{N_{CO_2}(r)}{N_{CO_2}(r) + N_{PEG}(r) + N_{solute}(r)} \quad (2)$$

and $N_i(r)$ is the number of interaction sites from a molecule of type i within a sphere of radius r around the COM of a solute, intramolecular sites excluded.

As can be seen, all solutes at all concentrations show CO_2 enhancement peaking between 3 and 4 Å before dropping toward bulk values as r increases, where the bulk value uses the average composition of each system as given in Table 1. Also significant is that both POL and PNE are significantly lower than EB or OCT and that they are less than half of EB or OCT at approximately all equivalent CO_2 concentrations. Sharpness in the EB peak is likely due to its planar structure allowing a CO_2 close to the benzene ring. Note that cross-over for OCT at $\frac{2}{3}S$ for small r is likely due to a lack of statistics since the total number of sites tends to zero as r decreases, thus basing $x(r)$ on a small number of configurations; for example, at the peak of $r = 3.0$ Å, the total average number of sites is 0.013 and where the curve starts to fall between $\frac{1}{3}S$ and S (as should be expected) at 3.5 Å, the total number of sites is only 0.27. The general solvation picture to emerge is that while non-polar solutes prefer solvation primarily from CO_2, the polar solutes only have partial solvation from CO_2 and interact substantially with PEG. Finally, the largest increases in $x(r)$ for all solutes occurs from $\frac{1}{3}S$ to $\frac{2}{3}S$ with smaller changes from $\frac{2}{3}S$ to S, another indication of a solute's CO_2 solvation shell being mostly complete at $\frac{2}{3}S$.

4 Conclusions

There is little effect of the concentration of CO_2 on solubility of the non-polar solutes EB and OCT, which prefer a solvation shell primarily of CO_2. The solubility of POL and PNE increased by 11 and 27 %, respectively, going from neat PEG-600 to CO_2-saturated PEG. For POL, this is related to hydrogen bonding to more favorable PEG hydroxyl sites likely made possible by structural changes in the solvent environment due to increased amount of CO_2. For PNE, the increase is less specific and is related to a solvation shell filled partially by CO_2 and partially by polymer sites. The implications for CO_2 extraction of small molecules from PEG are that there is little impact for non-polar solutes, while for polar solutes, the use of CO_2, in enhancing their solubility in the PEG + CO_2 mixture, makes extraction slightly more difficult, though the solubility enhancement is not large.

Acknowledgments The authors gratefully acknowledge the Maine Space Grant Consortium Undergraduate Scholarship Program and the University of New England's College of Arts and Sciences Dean's office for support, J. Bellan and J.I. Siepmann for discussion, and the University of Minnesota Supercomputing Institute where the calculations were partially carried out.

References

1. Heldebrant DJ, Jessop PG (2003) J Am Chem Soc 125:5600–5601
2. Heldebrant DJ, Witt HN, Walsh SM, Ellis T, Rauscher J, Jessop PG (2006) Green Chem 8:807–815
3. Wang J-Q, Cai F, Wang E, He L-N (2007) Green Chem 9: 882–887
4. Wang J-L, He L-N, Dou X-Y, Wu F (2009) Aust J Chem 62: 917–920
5. Arai M, Fujita S-I, Shirai M (2009) J Supercrit Fluids 47:351–356
6. Donaldson ME, Draucker LC, Blasucci V, Liotta CL, Eckert CA (2009) Fluid Phase Equilib 277:81–86
7. Blasucci VM, Husain ZA, Fadhel AZ, Donaldson ME, Vyhmeister E, Pollet P, Liotta CL, Eckert CA (2010) J Phys Chem A 114:3932–3938
8. Weidner E, Wiesmet V, Knez Ž, Škerget M (1997) J Supercrit Fluids 10:139–147
9. Lopes JA, Gourgouillon D, Pereira PJ, Ramos AM, da Ponte MN (2000) J Supercrit Fluids 16:261-267
10. Wiesmet V, Weidner E, Behme S, Sadowski G, Arlt W (2000) J Supercrit Fluids 17:1–12
11. Guadagno T, Kazarian SG (2004) J Phys Chem B 108: 13995–13999
12. Stubbs JM (2011) Fluid Phase Equilib 305:76–82
13. Li X, Hou M, Han B, Wang X, Yang G, Zou L (2008) J Chem Eng Data 53:1216–1219
14. Martin MG, Siepmann JI (1998) J Phys Chem B 102:2569–2577
15. Wick CD, Martin MG, Siepmann JI (2000) J Phys Chem B 104: 8008–8016
16. Stubbs JM, Potoff JJ, Siepmann JI (2004) J Phys Chem B 108: 17596–17605
17. Potoff JJ, Siepmann JI (2001) AIChE J 47:1676–1682
18. Panagiotopoulos AZ (1987) Mol Phys 61:813–826
19. Panagiotopoulos AZ, Quirke N, Stapleton M, Tildesley DJ (1988) Mol Phys 63:527–545
20. Smit B, de Smedt P, Frenkel D (1989) Mol Phys 68:931–950
21. Allen MP, Tildesley DJ (1987) Computer simulations of liquids. Oxford University Press, Oxford
22. Siepmann JI (1990) Mol Phys 70:1145–1158
23. Siepmann JI, Frenkel D (1992) Mol Phys 75:59–70
24. Frenkel D, Mooij GCAM, Smit B (1992) J Phys Condens Matter 4:3053–3076
25. de Pablo JJ, Laso M, Suter UW (1992) J Chem Phys 96: 2395–2403
26. Wick CD, Siepmann JI (2000) Macromolecules 33:7207–7218
27. Prausnitz JM, Lichtenthaler RN, Gomes de Azevedo E (1999) Molecular thermodynamics of fluid-phase equilibria, 3rd edn. Prentice Hall, Englewood Cliffs, NJ
28. Anderson KE, Siepmann JI (2008) J Phys Chem B 112: 11374–11380
29. Pasquali I, Comi L, Pucciarelli F, Bettini R (2008) Int J Pharm 356:76–81